Research Article | Vol. 27, No. 4 | 18 Feb 2019 | OPTICS EXPRESS 4271
Optics EXPRESS

Quartz-enhanced photoacoustic sensor for ethylene detection implementing optimized custom tuning fork-based spectrophone

MARILENA GIGLIO,[1,2] ARIANNA ELEFANTE,[1] PIETRO PATIMISCO,[1,2] ANGELO SAMPAOLO,[1,2] FABRIZIO SGOBBA, [1] HUBERT ROSSMADL,[3] VERENA MACKOWIAK,[3] HONGPENG WU,[2] FRANK K. TITTEL,[4] LEI DONG,[2,5] AND VINCENZO SPAGNOLO [1,2,6]

[1]*PolySense Lab - Dipartimento Interateneo di Fisica, University and Politecnico of Bari, CNR-IFN Via Amendola 173, Bari, Italy*
[2]*State Key Laboratory of Quantum Optics and Quantum Optics Devices, Institute of Laser Spectroscopy, Shanxi University, Taiyuan 030006, China*
[3]*Thorlabs GmbH, Hans-Boeckler-Straße 6, 85221 Dachau, Germany*
[4]*Department of Electrical and Computer Engineering, Rice University, 6100 Main Street, Houston, TX 77005, USA*
[5]*donglei@sxu.edu.cn*
[6]*vincenzoluigi.spagnolo@poliba.it*

Abstract: The design and realization of two highly sensitive and easily interchangeable spectrophones based on custom quartz tuning forks, with a rectangular (S_1) or T-shaped (S_2) prongs geometry, is reported. The two spectrophones have been implemented in a QEPAS sensor for ethylene detection, employing a DFB-QCL emitting at 10.337 μm with an optical power of 74.2 mW. A comparison between their performances showed a signal-to-noise ratio 3.4 times higher when implementing the S_2 spectrophone. For the S_2-based sensor, a linear dependence of the QEPAS signal on ethylene concentration was demonstrated in the 5 ppm −100 ppm range. For a 10 s lock-in integration time, an ethylene minimum detection limit of 10 ppb was calculated.

© 2019 Optical Society of America under the terms of the OSA Open Access Publishing Agreement

1. Introduction

Trace gas detection finds applications in a wide variety of fields [1]: monitoring of ammonia, nitric oxide, volatile organic compounds (VOCs), ethylene and acetone in human breath to assist the early detection of diseases, such as asthma, cancer and diabetes [2]; the detection of greenhouse and polluting gases for environmental monitoring [3]; hydrocarbon detection for the prediction of production outputs and estimate reserves in the petrochemical industry [4]. Non-optical techniques for trace gas detection, such as gas chromatography, gas spectrometry and electrochemical sensing can be costly, bulky, slow or can suffer from hysteresis. Conversely, laser optical absorption based techniques are less costly, offering long-term stability, high compactness and sensitivity and can operate in real-time [5,6]. Laser absorption spectroscopy has been widely employed in the mid-infrared (mid-IR) spectral range, where the strongest absorption lines for several gas species are located. These absorption features are typically related to molecular ro-vibrational transitions. Photoacoustic spectroscopy (PAS) has been demonstrated as one of the most robust and sensitive trace gas optical detection techniques, capable of performing measurements at sub-parts-per-trillion (ppt) concentration levels [6–8]. PAS is based on the detection of sound waves generated by gas absorption of modulated optical radiation using a sensitive microphone and a resonant acoustic cell. In 2002, an alternative approach was proposed, exploiting a commercial high-quality factor quartz tuning fork (QTF) instead of microphone and resonant cell, named quartz-enhanced

#355870 https://doi.org/10.1364/OE.27.004271
Journal © 2019 Received 20 Dec 2018; revised 25 Jan 2019; accepted 27 Jan 2019; published 6 Feb 2019

Optics EXPRESS

photoacoustic spectroscopy (QEPAS) [9]. The use of spectrophones, comprising quartz tuning forks acoustically coupled with micro-resonator (mR) tubes to enhance the signal-to-noise ratio, allowed a significant reduction of the detection module volume and immunity to environmental noise, while guaranteeing a high detection sensitivity and selectivity [10,11]. In 2015, a first generation of custom quartz tuning forks with rectangular prong geometry was designed, realized and tested, allowing a study on the influence of the dimensions of a quartz tuning fork on the main physical parameters controlling the QEPAS sensing performance, namely the resonance frequency, the quality factor and the electrical resistance [12]. Based on this study, in 2018 a second generation of custom quartz tuning forks was designed to investigate different prong geometries, such as the prong spacing up to 1.5 mm or prongs with a T-shaped longitudinal cross section or rectangular grooves carved on the prongs' surfaces [13].

The possibility to customize the quartz tuning forks for QEPAS sensing applications by varying the prong geometry and size made QEPAS extremely versatile. Depending on the specific target gas, sensing application or laser source, QEPAS sensors can be designed, implementing an appropriately selected quartz tuning fork. For example, the performance of a QEPAS sensor can be improved by employing a quartz tuning fork with a resonance frequency of few kHz, when detecting gas species characterized by slow non-radiative relaxation rates, such as CO, CO_2 or NO [14,15]. If implementing quartz tuning forks with both fundamental and first overtone flexural mode resonance frequencies lower than 40 kHz, two approaches can be employed: the double antinode excited QEPAS (DAE-QEPAS), where the two antinodes of the quartz tuning fork first overtone mode are simultaneously excited by one laser source [16] to improve the single-gas detection sensitivity, and the dual-gas QEPAS, where two different lasers excite independently both flexural modes of the quartz tuning fork to simultaneously detect two gas species [17]. Large prong spacing (≥800μm) custom quartz tuning forks permit alignment tolerances to be relaxed and the development of QEPAS sensors employing no-commercial or no-conventional laser sources. These were the cases of: i) the extension of QEPAS to the THz spectral range, where the laser beam diameters are comparable with the prong spacing (300μm) of the standard quartz tuning fork [18]; ii) the implementation of a high power (<1 W) fiber-amplified near-IR laser source [19]; iii) the exploitation of the tunability range provided by a monolithic array of 32 distributed feedback-QCLs for QEPAS sensing of broadband absorbers [20].

In this work, starting from the analysis of the geometrical and physical parameters of the available two generations of custom quartz tuning forks, two spectrophones with similar sizes were realized. In this way, we were able to design a QEPAS setup including a single acoustic detection module capable to accommodate two different spectrophones. Therefore, a quick switch between the two spectrophones was possible, requiring only a slight alignment after replacement. The performance of the two spectrophones were tested to detect ethylene (C_2H_4) in the mid-infrared spectral range. Ethylene detection is fundamental for its rising demand in the petrochemical industry as well as for air quality monitoring, fruit storage and transportation environment monitoring in food industry, and for inflammatory diseases diagnosis in medicine [21–25]. Depending on the application, the required ethylene detection sensitivity can vary from 1 ppm down to 10 ppb: climacteric fruits ripening and resulting early epinasty are triggered by concentrations in the 0.025-1 ppm range [26]; emissions from industrial facilities are regulated at less than 1 ppm [27]; a threshold of 10 ppb in air is considered a pollutant for plants [28] and traces of ethylene in the range of 10 ppb in breath are indicative of lipid peroxidation in lung epithelium [29]. In 2009, a near-infrared QEPAS-based sensor for ethylene detection was demonstrated, exhibiting a sensitivity of 0.5 ppm for 70 s integration time [30]. A mid-infrared QEPAS-based sensor was demonstrated in 2016, achieving a minimum detection limit (MDL) of 50 ppb in 70 s targeting an absorption line falling at 10.53 μm [31]. Recently, this MDL was lowered to 8 ppb at an integration time of 90 s, operating the sensor at pressures lower than 200 torr [32]. In this work, we demonstrate

Optics EXPRESS

that the accurate selection of the employed spectrophone with a specific quartz tuning fork geometry allows the realization of a QEPAS sensor with a minimum detection limit of lower than 10 ppb achievable in shorter integration times, which is suitable for all the above listed applications.

2. Spectrophones design and electrical characterization

The performance of two spectrophones were compared employing tuning forks from the two generations of custom quartz tuning forks realized so far. The two quartz tuning forks were selected in order to allow realizing two interchangeable spectrophones of the same size and provide a QEPAS signal as large as possible. Hence, both spectrophones can be accommodated and easily interchanged within the same acoustic detection module, consisting of a vacuum-tight gas cell equipped with two ZnSe windows antireflection (AR) coated in the 7-12 μm spectral range and gas-in and gas-out connectors. All 2nd generation custom quartz tuning forks have a total height of 14.1 mm, as reported in Table 1, with a prong length of 9 mm. Among them, QTF-S08-T, having *T-shaped* cross section-prongs, exhibited the largest QEPAS signal [13]. The QTF-S08-T acoustically coupled with two 12.4 mm-long tubes with internal diameter of 1.59 mm provided an increase of the signal-to-noise ratio (SNR) by a factor of 60 with respect to the bare tuning fork, representing a record for mid-IR QEPAS sensing [13]. Hence, this spectrophone was selected for this work and will be named hereafter as S_2.

In Table 1 the total height, the resonance frequency and quality factor of the fundamental and first overtone modes of the 1st generation of custom quartz tuning forks described in [33,34] are summarized and compared with QTF-S08-T, as reported in [13]. The surrounding air pressure at which the resonance parameters were measured are also reported.

Table 1. Total height (H), fundamental and first overtone flexural mode resonance frequency (f_0, f_1), and quality factor (Q_0, Q_1) of second- and first-generation QTFs and operation surrounding air pressure, as reported in [13] and [33,34], respectively.

	H (mm)	f_0 (Hz)	Q_0	f_1 (Hz)	Q_1	Air pressure (torr)	Ref.
Second generation QTF							
QTF-S08-T	14.1	12460.55	15540	_	_	760	[13]
First generation QTF							
QTF#1	27	2870.98	14668	17747.47	49488	50	[33,34]
QTF#2	14.7	7216.41	24520	41028.76	20630	50	[33,34]
QTF#3	15.4	3454.25	8538	21503.81	32850	50	[33,34]

Considering the constraint in the height imposed by S_2, among the 1st generations of custom quartz tuning forks, QTF#2 and QTF#3 have a total height comparable with S_2. The selection between these two quartz tuning forks is determined by two requirements. First, the flexural mode resonance frequency to be exploited must not exceed 40 kHz for efficient sound generation within the absorbing gas. Hence, the first overtone mode of QTF#2 cannot be used. Second, the overall spectrophone dimensions, determined also by the length of the two mR tubes, must be equivalent to the S_2 mR ones. The optimal tube length maximizing the sensor response is correlated with the inverse of the generated sound frequency, matching the quartz tuning fork resonance frequency f_n, and its value is between $\lambda_s/4$ and $\lambda_s/2$, but closer to $\lambda_s/2$ [35], where $\lambda_s = v_s/f_n$ is the sound wavelength and $v_s = 343$ m/s is the speed of sound in air. Based on the resonance frequencies reported in Table 1, the fundamental mode of QTF#2 and QTF#3 should require two tubes with lengths in the range 11.8 mm – 23.7 mm and 29.8 mm – 59.6 mm, respectively, which are unpractical ranges for an easy optical alignment. Based on the listed conditions, the best selection is QTF#3 operated at the first overtone flexural mode. The spectrophone S_1 was thus composed of QTF#3 and two 4.0 mm-long micro-resonator tubes with an internal diameter of 0.84 mm. In Table 2 the dimensions of

Optics EXPRESS

quartz tuning forks and mR tubes comprising the two spectrophones S_1 and S_2, as shown in Fig. 1(a), are summarized.

Table 2. Prongs' length L_{prong}, thickness T_{prong} and spacing s_{prong} of the QTF and length L_{tube} and inner diameter ID_{tube} of the mR tubes composing the two spectrophones.

Spectrophone	L_{prong} (mm)	T_{prong} (mm)	s_{prong} (mm)	L_{tube} (mm)	ID_{tube} (mm)
S_1	11.0	0.5	0.6	4.0	0.84
S_2	9.4	2	0.8	12.4	1.59

A sketch of the two spectrophones is shown in Fig. 1(a), where the S_1 mR tubes are positioned 5.8 mm below the top of the prong, close to the position of the second antinode of the QTF#3 first overtone mode, spaced 50 μm from the quartz tuning fork surface, while the S_2 tubes are placed at a distance of 200 μm from the QTF-S08-T surface, 2 mm below the top of the prong, as already discussed in [33]. The proper selection of the two quartz tuning forks allowed the realization of two interchangeable spectrophones to be hosted in the same acoustic detection module, depicted in Fig. 1(b), allowing the laser beam to be focused between the two quartz tuning forks prongs and through the related mRs with slight vertical adjustments. A cylindrical cavity having a height of 24 mm and a diameter of 13 mm is drilled inside the acoustic detection module in order to host S_1 or S_2, alternately.

The electrical properties of the described spectrophones were studied by using an experimental setup depicted in Fig. 1(b).

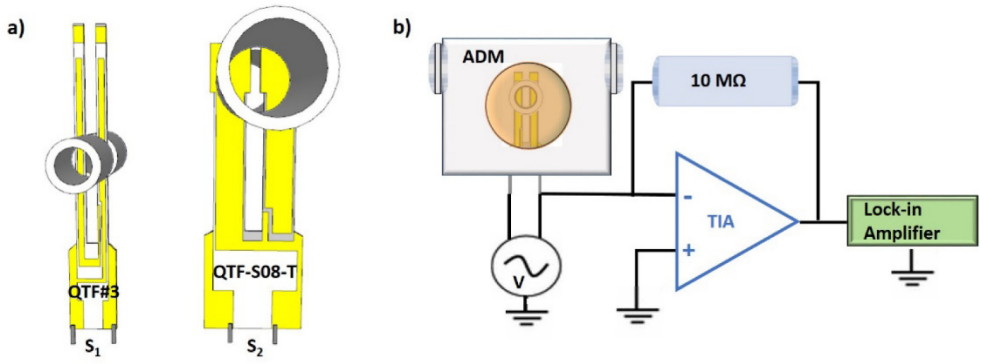

Fig. 1. Schematic of S_1 and S_2 spectrophones (a) and experimental setup for electrical characterization (b). V – sinusoidal Voltage; TIA – Transimpedance amplifier; ADM – Acoustic Detection Module.

The resonance properties of the two spectrophones were analysed by applying a sinusoidal voltage excitation with an amplitude of 170 mV. The quartz tuning fork current signal was transduced in a voltage signal by a custom-designed low-noise transimpedance amplifier employing a 10 MΩ feedback resistor and demodulated by a lock-in amplifier. The electrical responses of S_1 and S_2 at 120 Torr when the quartz tuning forks vibrate at the first overtone and fundamental flexural mode, respectively, are reported in Fig. 2.

Optics EXPRESS

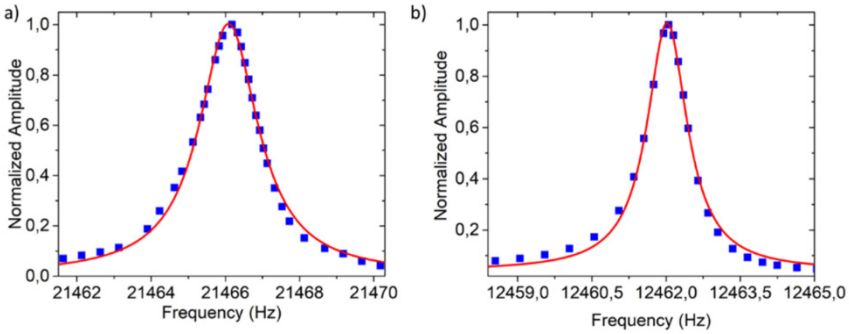

Fig. 2. Normalized resonance curves (blue squares) of the spectrophone S_1 employing QTF #3 (a) and S_2 employing QTF-S08-T (b) at 120 Torr. The red solid curves are the best Lorentzian fit [36].

For each spectrophone, the quartz tuning fork resonance frequency and quality factor were determined by fitting the acquired resonance spectra with Lorentzian curves. The Lorentzian fit of the S_1 curve exhibited a maximum at 21466.12 Hz, with a full width high maximum of 1.02 Hz, leading to a Q-factor of 20880, whereas, for S_2 a resonance frequency of 12462.02 Hz with a Q factor of 12530 was measured.

3. QEPAS measurements

The two spectrophones were implemented in the same QEPAS-based sensor, whose architecture is depicted in Fig. 3.

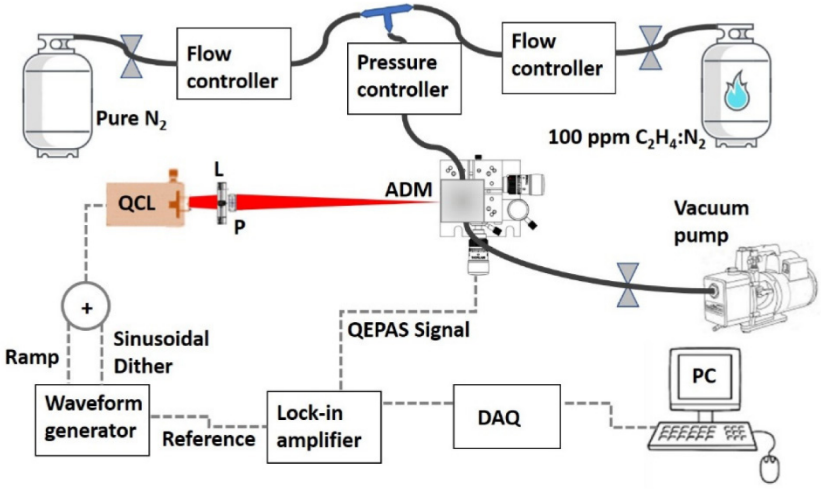

Fig. 3. Schematic of the QEPAS sensor for ethylene detection. QCL – Quantum Cascade laser; L – Lens; P – Pinhole; ADM – Acoustic Detection Module; DAQ – Data Acquisition board; PC – Personal Computer.

A distributed-feedback quantum cascade laser emitting at ~10.337 μm (Thorlabs, Inc., model QD10337HHLAS) was used as the laser source exciting the ethylene molecules within the acoustic detection module. With an injected current of 441.8 mA, the optical power measured with a pyroelectric power meter at the HHL output was 74.2 mW. The laser beam was focused into the acoustic detection module, fixed on a five-axis stage for alignment purposes, by using a 75 mm focal length ZnSe lens with a 7-12 μm AR coating. Such a focal length was chosen to achieve a tradeoff between the need for a small-diameter beam focused between the QTF#3 prongs of S_1 (S_{prong} = 0.6 mm) and a small numerical aperture of the same

Optics EXPRESS

beam passing through the 24.8 mm-long S_2 dual-tube micro-resonator. A ~2 mm diameter pinhole was placed between the lens and the acoustic detection module to cut the beam tails that could hit the mR tubes and/or the quartz tuning fork prongs, avoiding in this way an increase of a non-zero background that would worsen the sensor ultimate detection sensitivity. The far field spatial intensity distribution of the laser beam in the focal plane of the focusing lens was acquired using a pyroelectric camera (pixel size 100μm x 100μm). The use of a pinhole results in a focused beam diameter of 0.29 mm, well below the prong spacing of the employed quartz tuning forks (0.6 mm for S_1 and 0.8 mm for S_2). A ~7% optical power reduction was measured, with an optical power focused inside the acoustic detection module of P = 61.6 mW. QEPAS measurements were performed using the wavelength modulation and dual-frequency detection method: a sinusoidal dither matching half of the quartz tuning fork resonance frequency of the employed spectrophone was applied to the QCL current driver and the transduced quartz tuning fork signal was demodulated by the lock-in amplifier at the quartz tuning fork resonance frequency. The lock-in integration time was set at 100 ms. The demodulated signal was thus digitized and stored on a personal computer by means of a data acquisition board, with the card sampling time set at 3 times the lock-in integration time.

The first measurements were performed using spectrophone S_1. With the best alignment conditions, 97% of the laser power was measured to pass through the micro-resonator tubes and between the prongs. Preliminary measurements were conducted to identify the strongest absorption line falling within the tunability range of the QCL and the gas pressure and laser modulation amplitude providing the highest SNR. A wide-range spectral scan was performed while a certified concentration of 100 part-per-million (ppm) of C_2H_4:N_2 passed through the system with a controlled rate of 30 sccm. Furthermore, at a laser operating temperature of 15°C, the laser injection current was swept by adding a voltage ramp to the sinusoidal dither, with 2.1 V amplitude and 3 mHz frequency. The gas pressure and laser modulation amplitude voltage were varied in order to obtain the largest QEPAS signal, while maintaining the noise low. The optimal values resulted 120 Torr and 23 mV, respectively. In Fig. 4, a comparison between the absorption cross section simulated by using the HITRAN database [37] and the scan obtained by employing the spectrophone S_1 is shown.

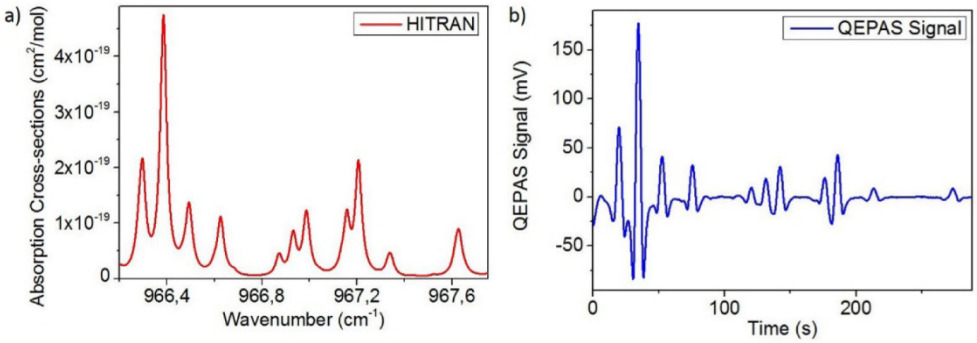

Fig. 4. 100 ppm C_2H_4:N_2 absorption spectrum simulated by using HITRAN database (a) and QEPAS spectral scan obtained at the same concentration over the QCL tunability range acquired by employing the spectrophone S_1 (b).

The comparison between the two graphs in Fig. 4 shows a very good correspondence between the simulated data and the acquired QEPAS spectral scan. In the investigated spectral range, the line located at 966.38 cm^{-1} is the strongest C_2H_4 absorption feature with a linestrength of $2.21 \cdot 10^{-20}$ cm/mol. A narrower spectral scan around the largest intensity absorption peak was recorded by applying a ramp with an amplitude of 300 mV and a frequency of 10 mHz to the QCL current driver. The obtained QEPAS spectrum is shown in Fig. 5 (green line). The spectrophone S_1 was subsequently replaced with S_2. After realigning

Optics EXPRESS

the system, by slightly adjusting the laser beam vertical position, a 97.9% power transmission through the acoustic detection module was measured, slightly higher than with S_1, justified by the larger QTF-S08-T prong spacing (800 μm) and the tubes' internal diameter. The spectral scan of the 966.38 cm^{-1} absorption peak for 100 ppm of C_2H_4:N_2 acquired by employing S_2 is shown in Fig. 5 (orange line), obtained by using the same operating conditions as for S_1.

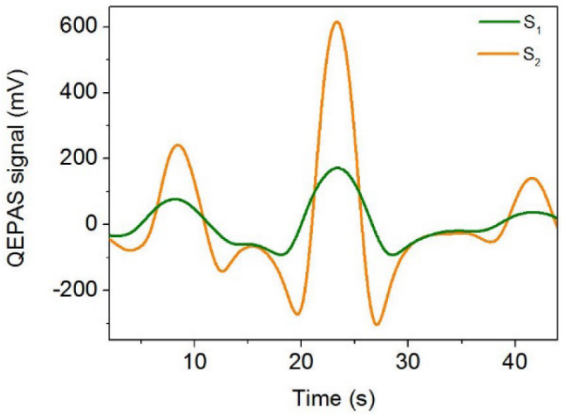

Fig. 5. QEPAS signal of 100 ppm C_2H_4:N_2 acquired when S_1 (orange solid line) or S_2 (green solid line) are implemented in the system. Both spectra were acquired at 100 ms lock-in integration time.

The ethylene peak signal, measured by implementing the spectrophone S_1 in the acoustic detection module, was 175.8 mV, with a 1σ noise of 0.175 mV, leading to a signal-to-noise ratio (SNR) of ~1000 and an SNR = 1 minimum detection limit of ~100 part-per-billion (ppb). When implementing the spectrophone S_2, a signal of 615.8 mV, with a 1σ noise of 0.180 mV, was obtained. The similar noise values measured with the two spectrophones, as well as the similar values of the optical power transmitted through the spectrophones, confirmed that the accurate selection of the implemented quartz tuning forks, together with the proper selection of the lens focal length, allows the assembly of two interchangeable spectrophones that can be set in the same acoustic detection module. Although showing a comparable noise, the spectrophone S_2 provides an SNR of 3420, ~3.4 times higher than the one obtained by employing the spectrophone S_1. Despite that S_1 exhibited a higher quality factor, lowering the resonance frequency from 21.4 kHz (S_1) down to 12.4 kHz in S_2 together with the record sound amplification obtained for S_2 [13] lead to an improvement of the sensor performance when implementing S_2. An ethylene MDL of ~30 ppb was achieved. Then, a S_2-based QEPAS sensor calibration was performed. Figure 6(a) shows the QEPAS spectral scans measured for 40 ppm, 30 ppm, 20 ppm, 10 ppm and 5 ppm of C_2H_4:N_2 obtained by diluting ethylene with pure N_2. The signal acquired in pure N_2 is also shown for comparison. The peak values were extracted from each spectral scan in Figs. 5 and 6(a) and plotted as a function of the ethylene concentration in Fig. 6(b).

Optics EXPRESS

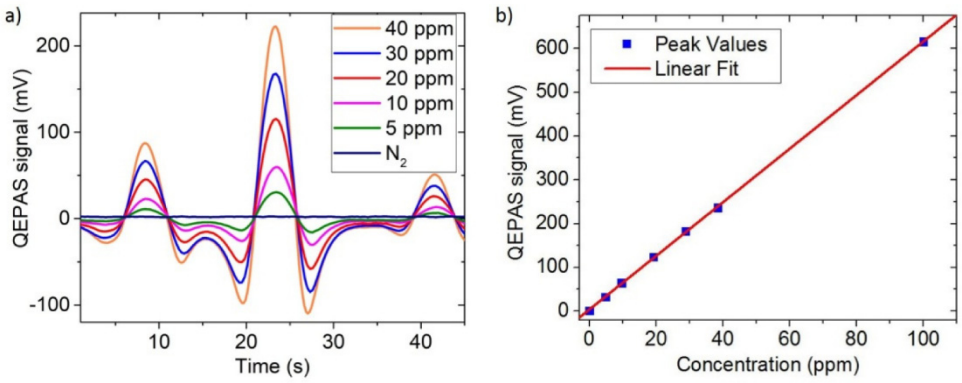

Fig. 6. QEPAS spectral scans measured for (a) 40 ppm, 30 ppm, 20 ppm, 10 ppm and 5 ppm C_2H_4:N_2 and pure N_2 and peak values (b) measured for each ethylene concentration (blue squares) with the corresponding best linear fit (red line).

By linearly fitting the peak values as a function of the ethylene concentration, a calibration curve was obtained. The linear fit yields a slope of 6.12 mV/ppm, with an intercept of 4 mV, comparable with the 1.2 mV background noise level measured in pure N_2. The calculated R-squared value is equal to 0.999.

The 1σ noise can be lowered by further averaging the signal over longer times [38]. An Allan-Werle deviation analysis was performed with the aim of estimating the 1σ noise (and thus the achievable minimum detection limit) as a function of the lock-in integration time. The obtained Allan-Werle deviation plot is reported in Fig. 7.

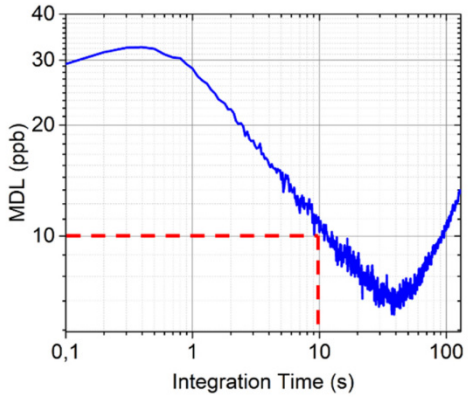

Fig. 7. Allan-Werle deviation plot of the QEPAS signal in ppb units as a function of the lock-in integration time. For a 10 s integration time, a minimum detection limit of ~10 ppb was achieved (red dashed line).

For a lock-in integration time of 10 seconds a minimum detection limit as low as 10 ppb was achieved. This detection sensitivity improved to 7 ppb by increasing the integration up to 30 second. For longer integration times, drift effects emerge, induced by the mechanical instability mainly caused by the vacuum pump, and the sensor performance deteriorates. A future improvement of the sensor long term stability can be obtained by employing low-vibration pump. However, the achieved sensitivity level using the S_2-based QEPAS sensor fulfills the requirements for ethylene detection in the food industry, pollution monitoring and breath sensing.

Optics EXPRESS

4. Conclusions

In this work we designed and realized two interchangeable custom quartz tuning fork-based spectrophones, namely S_1 and S_2, capable of high QEPAS sensing performance. The implemented quartz tuning forks were selected among the two different custom quartz tuning forks generations realized so far, in order to assemble two spectrophones having equivalent sizes. The performances of S_1 and S_2 were tested in a QEPAS-based sensor for ethylene detection, designed to easily allow switching of the two spectrophones. At 100 ppm C_2H_4:N_2 concentration and 100 ms integration time, S_2 provided a QEPAS signal ~3.4 times higher than that measured using S_1. This result shows that an appropriate design of the quartz tuning fork as well as its acoustic coupling with resonator tubes can efficiently improve the ultimate performance of a QEPAS sensor. The performance of the ethylene S_2-based QEPAS sensor was investigated in detail, by calibrating the sensing system and determining its ultimate detection sensitivity. For a lock-in integration time of 10 s, a minimum detection limit of 10 ppb was estimated, making the sensor suitable for the detection sensitivity required in breath sensing, air quality control and fruit transportation control.

Funding

Welch Foundation (C0568); National Natural Science Foundation of China (NSFC) (61622503, 61575113, 61805132); Ministry of Education of the People's Republic of China, 111 project (D18001).

Acknowledgments

The authors from Dipartimento Interateneo di Fisica di Bari acknowledge financial support from THORLABS GmbH, within the joint-research laboratory PolySense.

References

1. J. Hodgkinson and R. P. Tatam, "Optical gas sensing: a review," Meas. Sci. Technol. **24**(1), 012004 (2013).
2. D. Smith and P. Španěl, "The challenge of breath analysis for clinical diagnosis and therapeutic monitoring," Analyst (Lond.) **132**(5), 390–396 (2007).
3. P. Daukantas, "Air-quality monitoring in the mid-infrared," Opt. Photonics News **26**(11), 26–33 (2015).
4. J. G. Speight, *The Chemistry and Technology of Petroleum* (CRC Taylor & Francis Group, 2014).
5. I. Galli, S. Bartalini, S. Borri, P. Cancio, D. Mazzotti, P. De Natale, and G. Giusfredi, "Molecular gas sensing below parts per trillion: radiocarbon-dioxide optical detection," Phys. Rev. Lett. **107**(27), 270802 (2011).
6. T. Tomberg, M. Vainio, T. Hieta, and L. Halonen, "Sub-parts-per-trillion level sensitivity in trace gas detection by cantilever-enhanced photo-acoustic spectroscopy," Sci. Rep. **8**(1), 1848 (2018).
7. M. W. Sigrist, "Trace gas monitoring by laser-photoacoustic spectroscopy," Infrared Phys. Technol. **36**(1), 415–425 (1995).
8. L. Xiong, W. Bai, F. Chen, X. Zhao, F. Yu, and G. J. Diebold, "Photoacoustic trace detection of gases at the parts-per-quadrillion level with a moving optical grating," Proc. Natl. Acad. Sci. U.S.A. **114**(28), 7246–7249 (2017).
9. P. Patimisco, A. Sampaolo, L. Dong, F. K. Tittel, and V. Spagnolo, "Recent advances in quartz enhanced photoacoustic sensing," Appl. Phys. Rev. **5**(1), 011106 (2018).
10. A. Sampaolo, S. Csutak, P. Patimisco, M. Giglio, G. Menduni, V. Passaro, F. K. Tittel, M. Deffenbaugh, and V. Spagnolo, "Methane, ethane and propane detection using a compact quartz enhanced photoacoustic sensor and a single interband cascade laser," Sensor Actuat. Biol. Chem. **282**, 952–960 (2019).
11. A. Sampaolo, P. Patimisco, M. Giglio, L. Chieco, G. Scamarcio, F. K. Tittel, and V. Spagnolo, "Highly sensitive gas leak detector based on a quartz-enhanced photoacoustic SF_6 sensor," Opt. Express **24**(14), 15872–15881 (2016).
12. P. Patimisco, A. Sampaolo, L. Dong, M. Giglio, G. Scamarcio, F. K. Tittel, and V. Spagnolo, "Analysis of the electro-elastic properties of custom quartz tuning forks for optoacoustic gas sensing," Sensor Actuat. Biol. Chem. **227**, 539–546 (2016).
13. P. Patimisco, A. Sampaolo, M. Giglio, S. Dello Russo, V. Mackowiak, H. Rossmadl, A. Cable, F. K. Tittel, and V. Spagnolo, "Tuning forks with optimized geometries for quartz-enhanced photoacoustic spectroscopy," Opt. Express **27**(2), 1401–1415 (2019).
14. Y. Ma, Y. He, X. Yu, C. Chen, R. Sun, and F. K. Tittel, "HCl ppb-level detection based on QEPAS sensor using a low resonance frequency quartz tuning fork," Sensor Actuat. Biol. Chem. **233**, 388–393 (2016).
15. G. Wysocki, A. A. Kosterev, and F. K. Tittel, "Influence of molecular relaxation dynamics on quartz-enhanced photoacoustic detection of CO_2 at $\lambda = 2$ μm," Appl. Phys. B **85**(2-3), 301–306 (2006).

Optics EXPRESS

16. H. Zheng, L. Dong, P. Patimisco, H. Wu, A. Sampaolo, X. Yin, S. Li, W. Ma, L. Zhang, W. Yin, L. Xiao, V. Spagnolo, S. Jia, and F. K. Tittel, "Double antinode excited quartz-enhanced photoacoustic spectrophone," Appl. Phys. Lett. **110**(2), 021110 (2017).
17. H. Wu, X. Yin, L. Dong, K. Pei, A. Sampaolo, P. Patimisco, H. Zheng, W. Ma, L. Zhang, W. Yin, L. Xiao, V. Spagnolo, S. Jia, and F. K. Tittel, "Simultaneous dual-gas QEPAS detection based on a fundamental and overtone combined vibration of quartz tuning fork," Appl. Phys. Lett. **110**(12), 121104 (2017).
18. A. Sampaolo, P. Patimisco, M. Giglio, M. S. Vitiello, H. E. Beere, D. A. Ritchie, G. Scamarcio, F. K. Tittel, and V. Spagnolo, "Improved tuning fork for terahertz quartz-enhanced photoacoustic spectroscopy," Sensors (Basel) **16**(4), 439–446 (2016).
19. H. Wu, A. Sampaolo, L. Dong, P. Patimisco, X. Liu, H. Zheng, X. Yin, W. Ma, L. Zhang, W. Yin, V. Spagnolo, S. Jia, and F. K. Tittel, "Quartz enhanced photoacoustic H_2S gas sensor based on a fiber-amplifier source and a custom tuning fork with large prong spacing," Appl. Phys. Lett. **107**(11), 111104 (2015).
20. M. Giglio, P. Patimisco, A. Sampaolo, A. Zifarelli, R. Blanchard, C. Pfluegl, M. F. Witinski, D. Vakhshoori, F. K. Tittel, and V. Spagnolo, "Nitrous oxide quartz-enhanced photoacoustic detection employing a broadband distributed-feedback quantum cascade laser array," Appl. Phys. Lett. **113**(17), 171101 (2018).
21. H. Zimmermann, H. and R. Walzl, *Ethylene, Ullmann's Encyclopedia of Industrial Chemistry* (Wiley-VCH, 2009).
22. A. Tullo, "Petrochemicals: market will remain tight despite new capacity," Chem. Eng. News **96**, 29 (2018).
23. J. H. Seinfeld, "Urban air pollution: state of the science," Science **243**(4892), 745–752 (1989).
24. J. C. Pech, M. Bouzayen, and A. Latché, "Climacteric fruit ripening: ethylene-dependent and independent regulation of ripening pathways in melon fruit," Plant Sci. **175**(1-2), 114–120 (2008).
25. L. M. Paardekooper G. Bogaart, M. S. Kox, I. Dingjan, A. H. Neerincx, M. B. Bendix, M. Ter Beest, F. J. Harren, T. Risby, P. Pickkers, and N. Marczin, "Ethylene, an early marker of systemic inflammation in humans," Sci. Rep. **7**, 1–9 (2017).
26. S. P. Burg and E. A. Burg, "Role of ethylene in fruit ripening," Plant Physiol. **37**(2), 179–189 (1962).
27. ACGIH, *Threshold Limit Values for Chemical Substances and Physical Agents in the Workroom Environment* (ACGIH, 1986–1987).
28. F. B. Abeles and H. E. Heggestad, "Ethylene: an urban air pollutant," J. Air Pollut. Control Assoc. **23**(6), 517–521 (1973).
29. D. C. Dumitras, D. C. Dutu, C. Matei, A. M. Magureanu, M. Petrus, C. Popa, and M. Patachia, "Measurements of ethylene concentration by laser photoacoustic techniques with applications at breath analysis," Rom. Rep. Phys. **60**, 593–602 (2008).
30. S. Schilt, A. A. Kosterev, and F. K. Tittel, "Performance evaluation of a near infrared QEPAS based ethylene sensor," Appl. Phys. B **95**(4), 813–824 (2009).
31. Z. Wang, Z. Li, and W. Ren, "Quartz-enhanced photoacoustic detection of ethylene using a 10.5 μm quantum cascade laser," Opt. Express **24**(4), 4143–4154 (2016).
32. Z. Wang, J. Geng, and W. Ren, "Quartz-enhanced photoacoustic spectroscopy (QEPAS) detection of the ν_7 band of ethylene at low pressure with CO_2 interference analysis," Appl. Spectrosc. **71**(8), 1834–1841 (2017).
33. F. K. Tittel, A. Sampaolo, P. Patimisco, L. Dong, A. Geras, T. Starecki, and V. Spagnolo, "Analysis of overtone flexural modes operation in quartz-enhanced photoacoustic spectroscopy," Opt. Express **24**(6), A682–A692 (2016).
34. P. Patimisco, A. Sampaolo, V. Mackowiak, H. Rossmadl, A. Cable, F. K. Tittel, and V. Spagnolo, "Loss mechanisms determining the quality factors in quartz tuning forks vibrating at the fundamental and first overtone modes," IEEE Trans. Ultrason. Ferroelectr. Freq. Control **65**(10), 1951–1957 (2018).
35. P. Patimisco, A. Sampaolo, H. Zheng, L. Dong, F. K. Tittel, and V. Spagnolo, "Quartz–enhanced photoacoustic spectrophones exploiting custom tuning forks: a review," Adv. Phys. X **2**, 169–187 (2016).
36. Y. Qin and R. Reifenberger, "Calibrating a tuning fork for use as a scanning probe microscope force sensor," Rev. Sci. Instrum. **78**(6), 063704 (2007).
37. http://www.hitran.org/
38. M. Giglio, P. Patimisco, A. Sampaolo, G. Scamarcio, F. K. Tittel, and V. Spagnolo, "Allan deviation plot as a tool for quartz enhanced photoacoustic sensors noise analysis," IEEE Trans. Ultrason. Ferroelectr. Freq. Control **63**(4), 555–560 (2016).

193.204.188.118 {ts '2019-02-14 06:02:26'}